MEASURING BOLTED JOINT BEARING DEFORMATION AND STIFFNESS

B. Vangrimde [1], R.Boukhili [1]

[1] *Centre for Applied Research on Polymers, Ecole Polytechnique de Montréal, CP 6079, succursale Centre-Ville, Montréal, Quebec, H3C 3A7, Canada*

SUMMARY: This investigation deals with the stress-strain behaviour of single-bolt double shear bolted joints. The standard test method for bearing response of polymer matrix composite laminates (ASTM D5961) provides a way to measure bearing stress, bearing strain and bearing chord stiffness. Although the bearing strain is clearly defined, obtaining this strain from the measured data is not a straightforward procedure. It is shown that the tensile strain in the coupon, included in the measured data, profoundly influences the bearing strain and bearing chord stiffness. Data for 6 glass fibre-reinforced polyester laminates and 3 coupon geometries are presented. A simple correction procedure is proposed which allows the tensile strain to be excluded from the measured data. Experimental and finite element results are presented to provide insight for future experiments and to show that there is a merit in isolating the deformation caused by coupon tensile strain from the bearing deformation.

KEYWORDS: bolted joints, fastening, bearing deformation, bearing stiffness, GRP.

INTRODUCTION

Recently Camanho and Matthews [1] reviewed the active research domain of stress and strength analysis of bolted joints for composite structures. A popular case study is the single-bolt double shear geometry. Although this test can provide useful deformation and stiffness data, they are rarely commented upon. The standard test method for bearing response of polymer matrix composite laminates (ASTM D5961) provides a means to measure bearing strain and bearing chord stiffness. Our findings, specifically for the deformation and stiffness behaviour of six glass-fibre reinforced polyester laminates are reported in this paper.

As documented by EUROCOMP [2], the relative displacement of two joined plates consists of axial extension of the joined plates, fastener deflection in shear and bending and local bearing deformation of the holes. Other factors that will influence the relative displacement of the joined plates are the bolt-hole fit, head/tail restraints of the bolt and, in the case of single shear joints, fastener rigid body rotation.

The ASTM standard defines that the bearing strain (ε_{br}) is the ratio of the deformation "δ_1" of the bearing hole in the direction of the bearing load and the original diameter of the hole "D". Fig 1 shows the procedure proposed by ASTM for double shear joints: the relative displacement of the plates is measured by two LVDT displacement transducers. This

displacement "δ_L", measured at a distance "L" away from the centre of the hole, clearly includes the real bearing deformation of the test specimen hole, "δ_1", but also the deformation of the bolt, "δ_2", the extension of the tested coupon over a distance L-D/2 and the deformation of the loading plates between the hole centre and the attachment point of the LVDTs. This last deformation consists out of local bearing deformation of the plate holes and extension of the plates. If bending and rotation of the loading plates takes place, LVDT displacement readings will also be influenced. In order to isolate the real bearing strain, it is believed that the extent of the different displacement mechanisms should be assessed.

Fastener flexibility was already studied by Huth [3]. Metallic and graphite/epoxy joints were analysed under static and fatigue conditions. Big differences were found between previously proposed fastener flexibility models and a new formula was presented. Barrois [4] presented equations for bolt deflection. Shear deformation of the bolt was considered and different head/tail restraints for the bolt were taken into account. An elastic foundation was used to represent the load distribution on the bolt. Collings and Beauchamp [5] presented bearing deflection data for CFRP. Deflection was measured between the bolt and two points at a fixed distance beside the original hole centre. Only the change of bearing stiffness between different laminates was considered to be meaningful, not the absolute values. No damage was found for the initial linear part of the bearing stress-bearing strain curves.

Recently, Turvey [6] expressed the need for a preferred test configuration and a preferred joint extension measurement method. The ASTM standard formulates an appropriate solution for the first need but it will be shown in this paper that the joint extension measurement method needs to be further detailed.

EXPERIMENTAL SET-UP

According to the ASTM D5961 standard, the load was applied to the bearing coupon by means of a double shear clevis and the bearing deformation was monitored by LVDT displacement transducers attached on both sides of the specimen, as shown in Fig. 1. The bearing stress (σ_{br}) defined by Eqn 1 as the applied load "P" divided by the hole diameter and the thickness of the laminate "h" was monitored throughout the tests as well as the bearing strain (ε_{br}), defined by Eqn 2 as the average of the two LVDT displacements, "δ_a" and "δ_b", divided by the hole diameter.

$$\sigma_{br} = \frac{P}{D.h} \tag{1}$$

$$\varepsilon_{br} = \frac{\left(\delta_a + \delta_b\right)}{2.D} \tag{2}$$

The load was applied by an MTS 810 fatigue testing machine and the data was collected by Teststar II software. The laminates being tested were compression molded glass-fibre reinforced polyester laminates of 6.2 mm thick with a fibre volume fraction close to 40%. Table 1 shows the fibre contents and in-plane elastic properties. The experimental modulus ($E_{x,exp}$) is reported as are approximate laminate elastic properties obtained by classical lamination theory (CLT) and micromechanics equations. Since there is a good agreement between the experimental and the CLT longitudinal modulus, the CLT values are used for the finite element analysis (FEA).

Three different coupon geometries are studied to determine the influence of the coupon geometry on the stiffness and deformation behaviour:

- Standard specimen: w/D=6 e/D=3
- Long specimen: w/D=6 e/D=6
- Small specimen: w/D=2 e/D=3

Table 1: material composition and elastic constants

laminate	% 0° (%)	% 90° (%)	% mat (%)	$E_{x,\ exp.}$ (Gpa)	$E_{x,\ CLT}$ (Gpa)	$E_{y,\ CLT}$ (Gpa)	$G_{xy,\ CLT}$ (Gpa)	$\nu_{xy,CLT}$ (-)
A	63	0	37	26.9	25.5	11.3	3.91	0.36
B	34	34	32	21.1	19.6	19.6	3.95	0.20
C	0	0	100	15.9	15.9	15.9	5.66	0.405
D	38	0	62	23.2	21.6	13.5	4.62	0.38
E	33	9	58	21.3	20.5	15.3	4.6	0.33
F	56	9	35	-	24.2	13.3	3.92	0.30

The specimen geometry is defined by the pitch distance ratio w/D and the edge distance ratio e/D. The dimensions "w" and "e" are respectively the width of the coupon and the end distance. The latter is the distance from the centre of the hole to the non-loaded end of the coupon. A hole diameter of 9.53 mm and a bolt diameter of 9.23 mm were selected. Applied bolt torque was 3Nm. Washers with interior diameter 9.7 mm, exterior diameter 22.6 mm and a thickness of 2.5 mm were used between the tested coupons and the loading plates. The present coupon dimensions and laminate stacking sequences differ from those proposed by the ASTM standard but this does not make the present analysis inappropriate.

FINITE ELEMENT ANALYSIS OF BEARING DEFORMATION

Contrary to the ASTM standard for pin type bearing tests of metallic materials (ASTM E238), the standard for polymer matrix composite laminates does not specify that the bearing strain measurement shall be made in a way that it includes only a minimum of pin bending and tensile strain in the specimen. However, both are present for the proposed measuring method.

Since the tensile strain in the coupon is geometry and laminate lay-up dependent, it is most important, even for qualitative comparisons, that tensile strain induced deformation of the coupon is isolated from the bearing deflection. Since laminate thicknesses, washers or bolt constraints were not varied in this study, the bolt bending was believed to have only a quantitative and no qualitative influence on the results. Consequently, this paper will not focus on the bolt deformation. A finite element analysis (FEA) with Ansys software [7] was performed to analyse the deformation behaviour of the different laminates and coupon geometries. The bolt-hole clearance was modelled with contact elements since flexibility grows with bolt-hole clearance [4]. Point-to-surface contact elements (element number 48) were used to represent the bolt-hole contact. The bolt was considered to be rigid and the penalty function with Lagrange multipliers was found to be well-suited to avoid bolt-hole penetration. No friction was taken into account. The CLT elastic constants of Table 1 were used as orthotropic material properties. The elements used for the coupon were 4 node structural solid elements (element number 42). The simulation was in 2D, symmetry was used to reduce the model size and the hole was circumscribed by elements of only 0.1 mm high at every 2.8°. Since the bolt-hole contact area increases with the applied load, a non-linear analysis had to be performed.

Fig. 2 shows the finite element displacement results for a long coupon of laminate A. The bolt is at a fixed position and at the end of the coupon a 72 Mpa tensile stress is applied. For the section of the coupon at X=0, Fig. 2 shows that the bolt-hole contact point (X=0, Y=0) does not move in this analysis. However at the same section, the coupons' lateral edge (X=0, Y=28) does move 0.32 mm in the direction of the applied load. The discontinuous lines for the

X=4.8 mm section correspond to the hole centre. The section X=9.5 mm corresponds to the hole end. The hole end (X=9.5, Y=0) is therefore displaced by 0.33 mm. This displacement corresponds to the deformation of the bearing hole in the direction of the bearing load. It is the actual hole deformation "δ_1" that has to be measured to report a correct bearing strain. If the hole deformation is not read at this place but at a section 20 mm from the hole centre (X=24.8), the displacement varies from 0.35 in the centre to 0.36 mm at the sides: at least a 8 % difference with the real hole deformation. If a displacement "δ_L" is read by LVDTs at a section that is 70 mm from the hole centre (X= 74.8 mm), which is not excessive if the presence of washers and loading plates is considered, an almost uniform displacement of 0.50 mm would be read. This displacement "δ_L" is at least 52 % different from the real hole deformation "δ_1".

Fig. 3 and 4 compare the finite element displacement results for different coupon geometries and different laminates. Results are shown beginning from the hole end towards the loaded end of the plate for points lying on the symmetry axis. Therefore, the predicted hole deformation is the displacement at x=0. The displacement added to this value, along the x-axis is due to tensile coupon deformation and not to hole deformation. The applied stress was 72 MPa in all cases. Fig. 3 shows the displacement for different coupon geometries of laminate A. Finite element analysis predicts a different hole deformation "δ_1" for the different coupon geometries. This indicates that bearing chord stiffness will not only depend on width but also on end distance. Fig. 4 shows displacements of the long coupon for laminates A, B and C. Hole deformation is the lowest for the stiffest laminate, A. For laminates B and C however, the predicted hole deformations are very close. Since the longitudinal stiffnesses of B and C are far apart, it is clear that hole deformation cannot be characterised only by the longitudinal stiffness of the laminate. In both figures, the displacement plots are essentially linear, except close to the hole. Close to the hole there is a non-linear start where the longitudinal strains are low. The total curve can be approximated by an initial constant deformation part with zero longitudinal strain followed by a linear deformation part with constant strain. The extent of the zero-strain part, necessary to model the initial non-linear deformation, varies much with the geometry and far less with the laminate type. It is found to be close to D/2 for the long coupons, D/3 for the standard coupons and 7/8 D for the small coupons. This distance will be called X. The influence of the laminate type on the extent of the initial zero strain part will be neglected. The linear parts of the deformation plots correspond to a constant strain. This strain obeys the law of Hooke and can be calculated by dividing the stress applied on the coupon by the longitudinal modulus of the laminate. Consequently, when reading the displacement "δ_L" at a distance L away from the hole, the real bearing deformation can be approximated by subtracting the linear deformation part off the total deformation. The linear deformation acts over a distance (L - D/2 - X). This logical and simple formula, used to obtain an approximation "δ_{corr}" of the real bearing deformation "δ_1" is expressed by Eqn. 3.

$$\delta_{corr} = \delta_L - \frac{\sigma.(L - D/2 - X)}{E_x} \qquad (3)$$

Using this equation, the coupon extension part and hole deformation part can be uncoupled during bolt bearing tests. To verify the performance of the formula for the laminates and coupon geometries under investigation, FEA displacement results are summarised in Table 2. Laminates are listed from highest longitudinal stiffness to lowest longitudinal stiffness. The simulated LVDT position is taken 70 mm from the hole centre. The LVDT displacement is "δ_L", which differs from the real hole deformation by the amount (δ_L-δ_1)/δ_1. Table 2 shows that errors ranging from 52% to 116% are present, depending on laminate type and coupon geometry. When Eqn 3 is used, the corrected displacement δ_{corr} does

only differ from the real hole deformation by the amount $(\delta_{corr}-\delta_1)/\delta_1$. The predicted maximum error is only 3.2 % in this FEA study.

Table 2: Results of pin bearing deformation FEA and Eqn 3 (applied stress is 72 MPa).

Property/geometry		A	F	D	E	B	C
δ_L (mm)	Long	0.495	0.508	0.531	0.548	0.577	0.632
δ_1 (mm)		0.325	0.329	0.327	0.333	0.355	0.351
δ_{corr} (mm)		0.324	0.328	0.329	0.336	0.355	0.358
$(\delta_L-\delta_1)/\delta_1$ (%)		52	54	62	65	63	80
$(\delta_{corr}-\delta_1)/\delta_1$ (%)		-0.2	-0.3	0.7	0.8	0.0	2.0
δ_L (mm)	Standard	0.530	0.546	0.559	0.574	0.602	0.652
δ_1 (mm)		0.353	0.357	0.350	0.354	0.376	0.367
δ_{corr} (mm)		0.355	0.361	0.352	0.356	0.374	0.371
$(\delta_L-\delta_1)/\delta_1$ (%)		50	53	60	62	60	78
$(\delta_{corr}-\delta_1)/\delta_1$ (%)		0.5	1.2	0.6	0.6	-0.5	1.1
δ_L (mm)	Small	0.350	0.364	0.391	0.406	0.428	0.494
δ_1 (mm)		0.193	0.198	0.202	0.206	0.220	0.229
δ_{corr} (mm)		0.189	0.195	0.201	0.206	0.219	0.236
$(\delta_L-\delta_1)/\delta_1$ (%)		81	84	94	97	95	116
$(\delta_{corr}-\delta_1)/\delta_1$ (%)		-1.9	-1.7	-0.3	0.1	-0.5	3.2

Two remarks can be made about the correction:

1. FEA predicts that the correction results in a good approximation of the real bearing strain. Considering the scatter in experimental results, no further enhancement of the formula is sought. The small errors justify the definition of the distance X independent of laminate type. For transverse bearing tests, the definition of X has to be verified.
2. The finite element analysis considered a frictionless joint with a clearance of 3% (0.3 mm) between bolt and bolt hole. To verify the influence of these assumptions, other finite element analyses were performed considering perfect fit, bolt/hole friction and plate/washer friction (3D model). The friction coefficient was assumed to be 0.17 on all surfaces. Table 3 summarises the displacement results for a long coupon of laminate A. All assumptions do have an influence on the hole deformation δ_1 but the influence of friction assumptions on the coupon extension part $(\delta_L-\delta_1)$ is negligible. As a result, it is believed that the proposed correction can be used for pin bearing tests and bolt bearing tests with a small bolt torque.

Table 3: Displacements obtained by different model assumptions (laminate A, long coupon, applied stress is 72 MPa):

Conditions:	δ_1 (mm)	δ_L (mm)	$\delta_L-\delta_1$ (mm)
Clearance, no friction	0.325	0.495	0.170
no clearance, no friction	0.282	0.458	0.176
Clearance, bolt/hole friction	0.315	0.485	0.170
Clearance, bolt/hole and washer/coupon friction	0.305	0.475	0.170

EXPERIMENTAL BEARING DEFORMATION AND BEARING CHORD STIFFNESS

At least 3 coupons of every laminate and coupon geometry were tested during the experimental program. The distance "L" between LVDT reading point and hole centre varied between 70 and 80 mm and was measured for each test. Fig. 5 shows the transformation of the gathered load and displacement data to a bearing stress-bearing strain curve by using Eqn 1, 2 and 3. Eqn 3 is used in order to replace the total LVDT displacement, which results in the total strain curve, by the corrected displacement which results in the corrected bearing strain curve.

The left part of Fig. 5 shows that there is first a displacement of the LVDTs without a significant increase in force. It is the displacement needed to develop full contact between the bolt and the test specimen. From this point forward, the force and LVDT displacements develop similarly until 2 mm grip displacement where a damage mechanism causes the load to reduce and the LVDT displacements to increase instantaneously. The laminate does not fail catastrophically at this point and the loading continues up to 3 mm of grip displacement where total failure causes the load to drop and the LVDT displacements to increase suddenly. The same data is plotted on the right part of Fig. 5 together with 2 straight lines to measure the bearing chord stiffness. It is interesting to notice how damage signs are transformed into straight lines with a negative slope on the bearing stress-bearing strain curves.

Bearing chord stiffness "E_{br}" (Eqn 4) is defined by the standard as the ratio of the bearing stress difference "$\Delta\sigma_{br}$" over the bearing strain difference "$\Delta\varepsilon_{br}$" between two data points in the straight part of the bearing stress-bearing strain plot.

$$E_{br} = \Delta\sigma_{br} \Big/ \Delta\varepsilon_{br} \qquad (4)$$

For the tested specimens, the bearing chord stiffness was calculated between bearing stresses of 250 MPa and 100 MPa for the long and standard geometries and between 150 and 50 MPa for the small geometry. It is evident from Fig. 5 that the stiffness values for total and corrected strain plots vary considerably and that reported bearing strain offset strengths would also vary for the two cases.

A summary of the corrected bearing chord stiffness values with a 90% confidence interval is presented in Table 4. As in Table 2, the laminates are presented from the highest to the lowest longitudinal tensile modulus. It is clear that the bearing chord stiffness value for small coupons is less than for wide coupons. No distinction can be made for the end distance, contrary to FEA results in Table 2 which showed that a higher end distance would increase the stiffness. The general trend is that bearing chord stiffness reduces if the longitudinal modulus reduces. Collings and Beauchamp [5] reported however that the highest longitudinal tensile modulus does not coincide with the highest longitudinal bearing chord stiffness and the FEA results in Table 2 would agree on this argument.

Table 4: Experimental bearing chord stiffness values

	Long		Standard		Small	
	E_{br} (Mpa)	90% conf.. level (MPa-MPa)	E_{br} (Mpa)	90% conf. level (MPa-MPa)	E_{br} (Mpa)	90% conf. level (MPa-MPa)
A	9956	9248 - 10664	8482	7877 - 9087	6261	5915 - 6607
F	9209	8777 - 9641	9986	9105 - 10867	5903	5278 - 6528
D	9119	8558 - 9680	9292	8286 - 10298	5466	5104 - 5828
E	8857	8131 - 9583	8377	7723 - 9031	4961	4395 - 5527
B	8383	7921 - 8845	8095	7406 - 8784	4389	3724 - 5054
C	7414	7012 - 7816	7821	6701 - 8941	3883	3649 - 4117

FEA stiffness results are not presented since not enough data points were available close to the stress range where experimental stiffnesses were measured.

DISCUSSION

The ASTM D5961 standard does specify how, but not exactly where to measure the bearing strain. Fig. 2 shows that the position of the reading point on the coupon is in fact an important issue. Table 2 showed simulation results that indicated clearly that if the measured bearing strain is meant to be more than merely a vehicle to report the bearing stress data, corrections for the tensile strain present in the coupon have to be made. Eqn 3 is an attempt to correct the data. This formula was found by 2D frictionless FEA and should be verified by experiments. Although friction effects have an effect on the hole deformation, Table 3 indicated that friction does not influence the deformation induced by coupon tensile strain. Therefore, considering the good agreement shown in Table 2, the present formula can be used to isolate tensile strain in the coupon from real bearing strain. The formula uses one experimental value, the longitudinal modulus and one parameter determined by FEA, the zero-strain distance X. Bolt deformation is also present in the experiments but is laminate and coupon geometry independent as are the deformation and rotation of the loading plates. As a result the authors chose to correct only for the coupon extension being aware that the obtained strain and bearing chord stiffness values are not yet the real values, as they are defined. Nonetheless, the correction is a useful tool if different geometries or laminates have to be compared. Fig. 6 until 9 show that subtracting the coupon tensile deformation from the total deformation does permit to isolate the hole related effects. Fig 6 and 7 show respectively the bearing stress-total strain and the bearing stress-bearing strain curve for laminates A, B and C. In Fig. 6 a large stiffness difference is observed because of the strain in the coupon that is included. In Fig. 7 however, it is observed that the bearing chord stiffnesses of laminates A, B and C are very close. This can be very valuable: since the deformation by coupon tensile strain is eliminated, deformation of the hole and local damage around the hole are emphasised and isolated from the total response. Vangrimde and Boukhili [8] use this technique to analyse damage mechanisms in different laminates. Fig. 8 shows the bearing stress-total strain curves for laminate A. Since coupon widths are different, no real comparison can be made here between behaviour of standard and small coupons. When a bearing stress-bearing strain curve as in Fig. 9 is made, coupon width influences are eliminated and the real differences in bolt bearing response show up.

CONCLUSION

A simple method was discussed to isolate coupon tensile deformation from the total deformation that is measured during standard ASTM D5961 bolt bearing tests. As a consequence, a better estimate of the real bearing strain, as defined by the standard is obtained. The correction formula is adjusted to the present laminates and coupon geometries by a distance X, determined by FEA. Since no more laminate or coupon geometry dependent deformation is present after the correction, the real differences in bearing response of different coupon geometries and laminate stacking sequences can be observed. Reported bearing strains and bearing chord stiffness values are relative and not absolute since bolt bending effects and fixture deformation effects are still included in the corrected bearing strain. If measured bearing chord stiffness is to be made laboratory independent and useful for design, efforts are necessary to first assess and then isolate these effects from the measured deformation.

ACKNOWLEDGEMENTS

The authors wish to acknowledge the support given by the Natural Sciences and Engineering Research Council of Canada (NSERC) and the Quebec FCAR Fund (Formation de Chercheurs et Aide à la Recherche).

REFERENCES

1. Camanho , P.P. and Matthews, F.L., "Stress Analysis and Strength Prediction of Mechanically Fastened Joints in FRP: a Review", *Composites - Part A: Applied Science and Manufacturing*, Vol. 28, 1997, pp. 529-547.

2. Clarke, J.L., Ed., *Structural Design of Polymer Composites- EUROCOMP Design Code and Handbook*, E&FN Spon, London, 1996.

3. Huth, H., "Influence of Fastener Flexibility on the Prediction of Load Transfer and Fatigue Life for Multiple-Row Joints", *Fatigue in Mechanically Fastened Composite and Metallic Joints, ASTM STP 927,* Potter, J.M., Ed., American Society for Testing and Materials, Philadelphia, 1986, pp. 221-250.

4. Barrois, W., "Stresses and Displacements Due to Load Transfer by Fasteners in Structural Assemblies", *Engineering Fracture Mechanics*, Vol. 10, 1978, pp. 115-176.

5. Collings, T.A. and Beauchamp, M.J., "Bearing Deflection Behaviour of a Loaded Hole in CFRP", *Composites*, Vol. 15, 1984. pp. 33-38.

6. Turvey, G.J., "Single-bolt Tension Joint Tests on Pultruded GRP Plate - Effects of Tension Direction Relative to Pultrusion Direction", *Composite Structures*, Vol. 42, 1998, pp. 341-351.

7. ANSYS 5.3, SAS IP Inc., Houston, PA, 1996.

8. Vangrimde, B. and Boukhili, R., "Bolted Joint Fracture Modes in Glass-Fibre Reinforced Polyester", *Proceedings of the Twelfth International Conference on Composite Materials*, Paris, France, July 5-9, 1999.

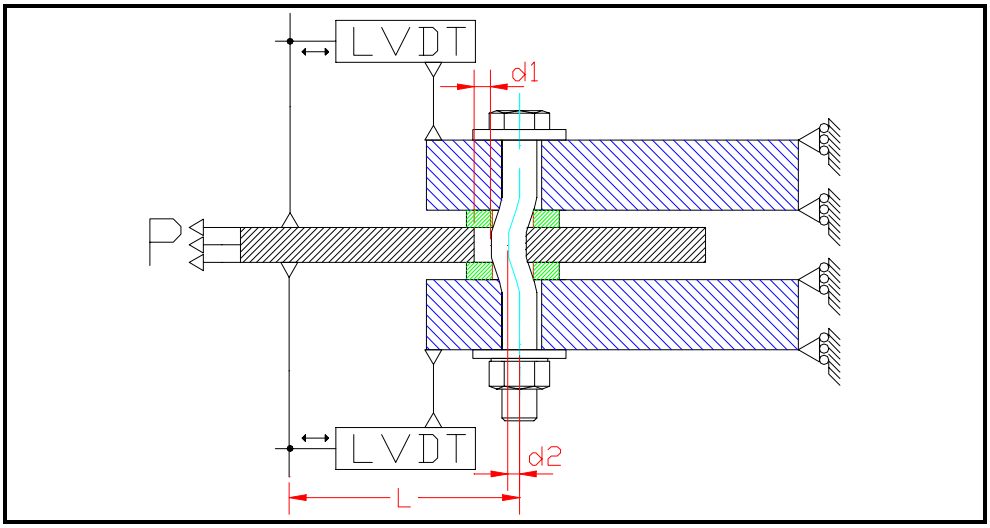

Fig. 1: Schematic presentation of single-bolt double shear bolted joint test.

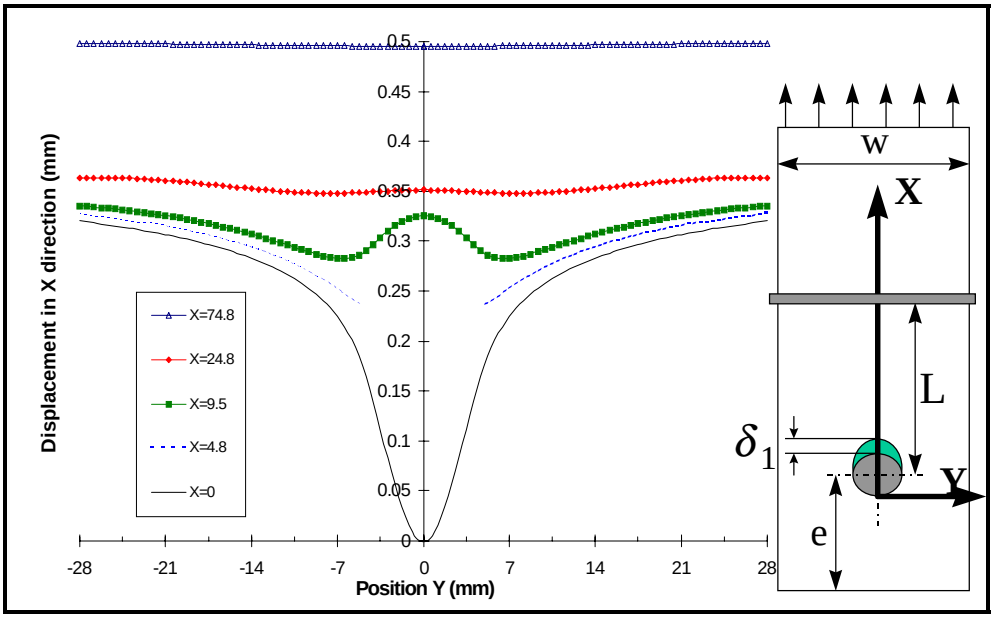

Fig. 2: FEA displacement results.

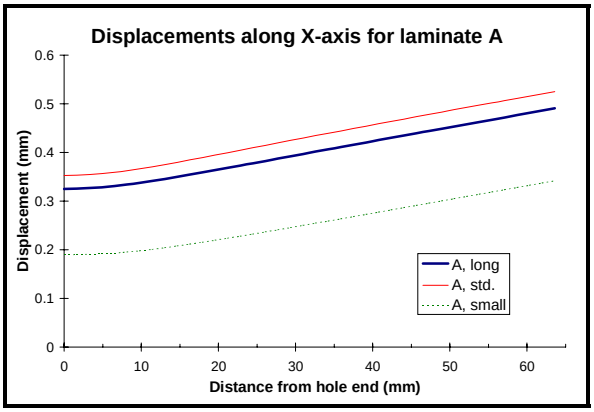

Fig. 3: FEA displacements for different coupon geometries

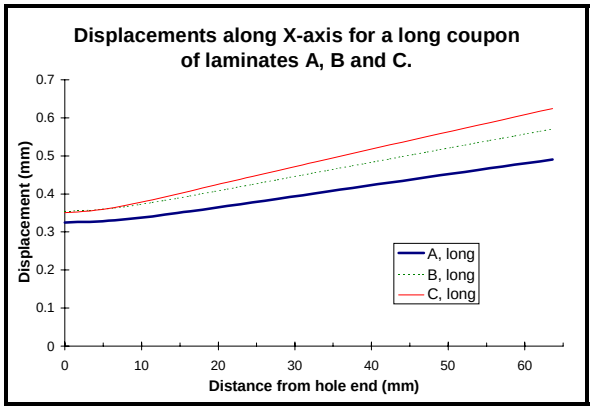

Fig. 4: FEA displacements for different laminates

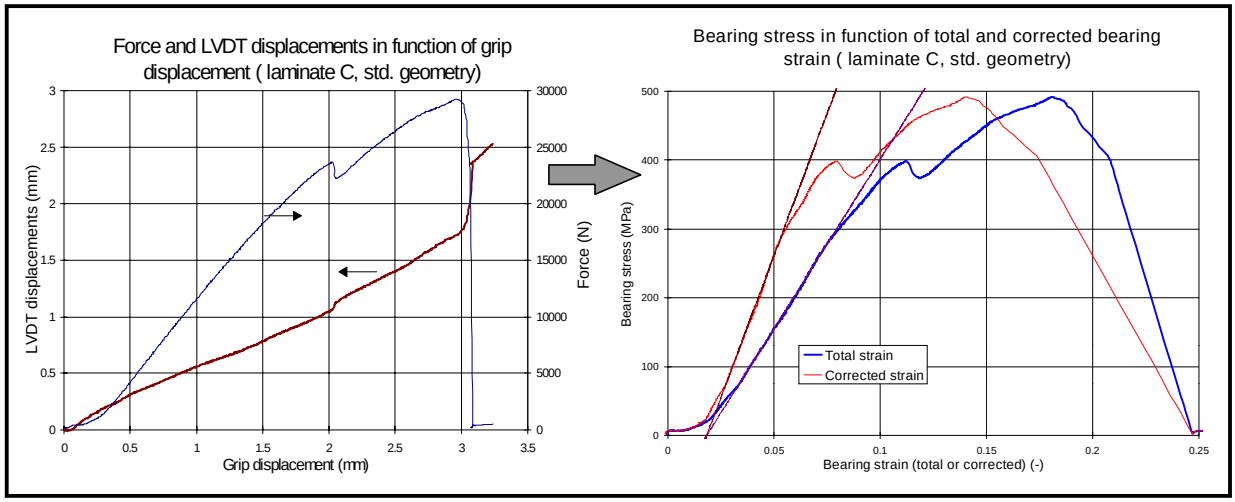

Fig. 5: Transformation of force and LVDT displacement data into bearing stress-bearing strain curves.

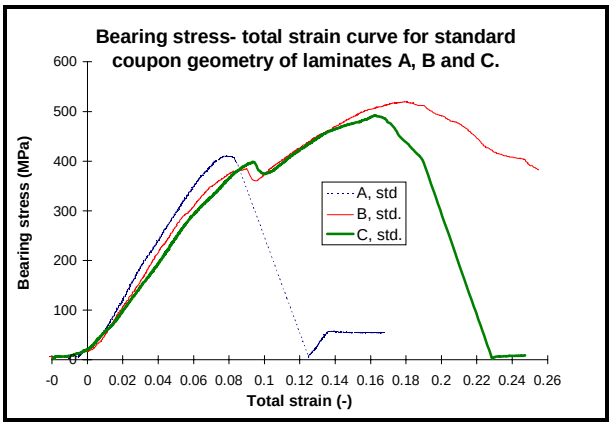

Fig. 6: Bearing stress-total strain curves for laminates A, B and C.

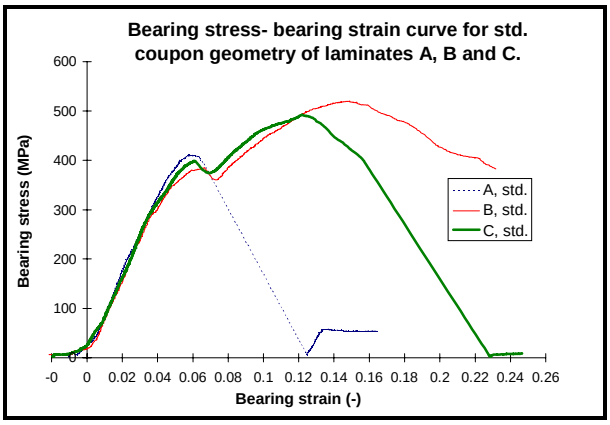

Fig. 7: Bearing stress-bearing strain curves for laminates A, B and C.

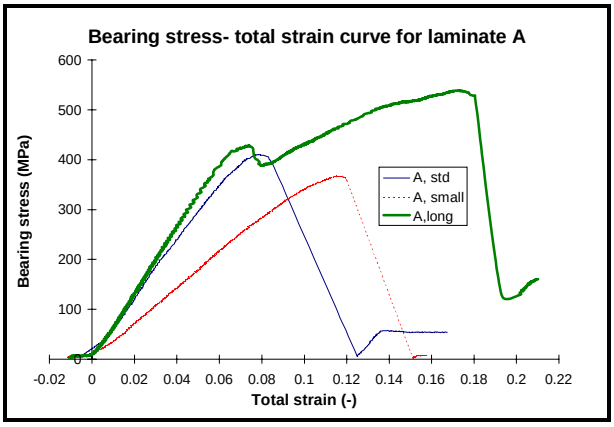

Fig. 8: Bearing stress-total strain curves for laminate A, different geometries.

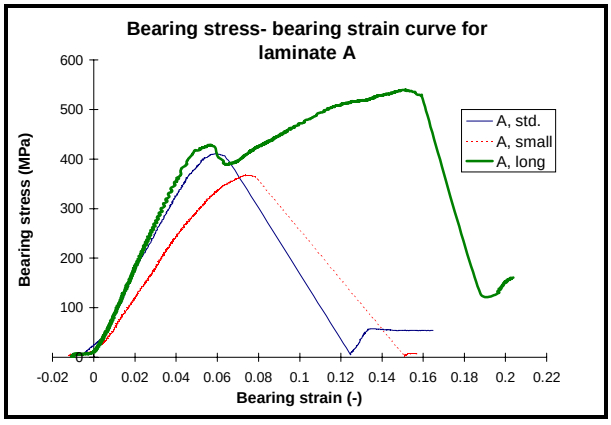

Fig. 9: Bearing stress-bearing strain curves for laminate A, different geometries.